Supplementary information to the "Localized Coherent Phonon Generation in Monolayer MoSe$_2$ from Ultrafast Exciton Trapping at Shallow Traps"

Soungmin Bae,[1,2*] Tae-Yong Jeong,[3] Hannes Raebiger,[2] Ki-Ju Yee,[3†] and Yong-Hoon Kim[1‡]

[1]*Department of Electrical Engineering, Korea Advanced Institute of Science and Technology (KAIST), Daejeon 34141, Korea*

[2]*Department of Physics, Yokohama National University, Yokohama, Japan*

[3]*Department of Physics, Chungnam National University, Daejeon, Korea*

CONTENTS

* Current address: Laboratory for Materials and Structures, Tokyo Institute of Technology, Yokohama 226-8503, Japan

† Correspondence email address: kyee@cnu.ac.kr

‡ Correspondence email address: y.h.kim@kaist.ac.kr

I. Experimental details and the reflectance spectra

Pump-probe experiments were performed using ultrashort optical pulses with a pulse duration of about 100 fs, which were generated from a mode locked Ti:sapphire oscillator with a repetition rate of 80 MHz. The center wavelength could be tuned in the wavelength range from 750 to 870 nm. Figure 1(a) of the manuscript shows the schematic of the pump-probe experiment setup. An optical pulse from the Ti:sapphire laser is divided into a strong pump pulse and a relatively weak probe pulse. In order to generate the time delay relative to the probe pulse, the pump pulse is reflected at a mirror mounted on a shaker which vibrates at a frequency of 13 Hz. We used an objective lens with a magnification of ×20 to overlap the pump and the probe beam spatially within the monolayer $MoSe_2$. A photodetector was used to measure the modulation of the probe transmittance induced by the pump pulse as a function of the time delay. The signal was accumulated with repeated scans until the noise could be reduced enough to reveal clear signal of coherent phonon oscillations. We performed the pump-probe experiments with changing the center wavelength of the optical pulse at a sample temperature of 80 K and a fixed pump fluence of about 150 $\mu J/cm^2$. The high-frequency modulation of the transmission change ($\Delta T/T$) corresponding to the CP signal was obtained by subtracting the slowly varying part that possibly originates from electronic contributions from the overall transient transmission change. The Fourier-transformation analysis of the transmission modulation was then carried out to obtain the frequency spectrum of generated coherent phonons.

In Fig. S1, we present the reflectance spectra of the defect-free (placed on and covered by hBN) and defective (on-quartz and unprotected) monolayer $MoSe_2$ samples. They exhibit absorption peaks at 1.63 eV and 1.60 eV, respectively, and, while the 1.63 eV peak from a pristine sample originates from A excitons (X_A), the 1.60 eV absorption peak appearing in defective $MoSe_2$ samples can be attributed to trions (X_{Trion}) possibly formed via the strong interaction between A excitons and the charges transferred from the quartz substrate ("charge puddles") and/or lattice defects.
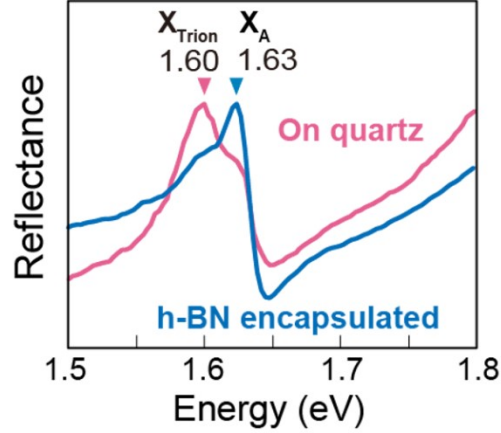
Fig. S1. Reflectance spectra of the defect-free (hBN encapsulated) and defective (on quartz) monolayer $MoSe_2$.

II. Computational details

Density functional theory (DFT) calculations were performed within the HSE06 hybrid functional [1] using the `VASP` code that implements the projector-augmented plane wave (PAW) method [2, 3]. The monolayer $MoSe_2$ models including a Se vacancy (V_{Se}), a defect complex of O adsorbed on Se vacancy (V_{Se}+O), and a defect complex of O_2 adsorbed on Se vacancy (V_{Se}+O_2) were modeled with a 8×8×1 $MoSe_2$ supercell with the Γ centered k-point sampling, and a Gaussian smearing of 0.02 eV is used. The defect-bound excitons trapped at V_{Se} and V_{Se}+O_2 defects were simulated using the occupation-constrained DFT or ΔSCF method with one electron from the highest occupied level promoted to the lowest unoccupied level and fixing the excited level occupations. The cell size dependence of occupation-constrained DFT calculation were verified for the V_{Se}+O_2 defect complex in monolayer $MoSe_2$ using the PBE generalized gradient approximation (GGA) functional [4]. The folded oscillator strength of the V_{Se}+O_2 defect center in monolayer $MoSe_2$ was obtained with the `VaspBandUnfolding` code [5]. Atomic structures and partial charge densities were visualized with the `VESTA` software. [6]

III. Convergence of the occupation constrained DFT calculation with respect to the cell size

The convergence of our occupation-constrained DFT calculations for excitons trapped at the $V_{Se}+O_2$ defect center in monolayer $MoSe_2$ with respect to supercell size has been tested using the PBE-GGA functional [4], and the results are summarized in Table S1. A Γ-centered 2×2×1-point grid was adopted for the 4×4×1 and 6×6×1 supercell and Γ point was used for 8×8×1 and 10×10×1 supercell. Density of states (DOS) and partial charge densities of in-gap defect states of the $V_{Se}+O_2$ in-gap defect states obtained from 4×4×1, 6×6×1 and 8×8×1 monolayer $MoSe_2$ supercell models are presented in Fig. S2. While the defect states of $V_{Se}+O_2$ in the 4×4×1 supercell model experience spurious interactions between periodic images and exhibit bandlike features, the $V_{Se}+O_2$ defect complex in the 6×6×1 and 8×8×1 supercell models exhibit localized characters with wavefunctions confined inside of supercells. Effective one-dimensional (1D) parameters characterizing the exciton trapping at $V_{Se}+O_2$ calculated with PBE-GGA functional (see Table S1) exhibit a similar convergent behavior, which indicates that the 8×8×1 supercell is sufficient to obtain the accurate phonon energy within the 0.1 meV (= 0.02 THz) accuracy. Comparing the PBE-GGA and HSE06 results obtained from the 8×8×1 supercell, we find that, in addition to the large band gap underestimation of PBE-GGA functional, both the atomic distortion ΔQ and the relaxation energy ΔE from PBE-GGA are smaller than those of the HSE06 functional. The trend for the HSE06 functional to predict more strongly localized states for the $V_{Se}+O_2$ defect complex

Table S1. Effective 1D parameters for the exciton trapped at the $V_{Se}+O_2$ defect complex in monolayer $MoSe_2$ calculated at various cell sizes with the PBE-GGA and HSE06 exchange-correlation functionals. Relaxation energies ΔE (eV), generalized configuration coordinates ΔQ (amu$^{1/2}$·bohr), effective phonon energies $\hbar\Omega$ (meV) and Huang-Rhys factors S defined as $S = \Delta E/\hbar\Omega$ are given.

	ΔE (eV)	ΔQ (amu$^{1/2}$·bohr)	$\hbar\Omega$ (meV)	S
PBE-GGA (4×4×1)	0.195	5.02	15.26 (3.67 THz)	12.8
PBE-GGA (6×6×1)	0.100	3.33	16.45 (3.98 THz)	6.1
PBE-GGA (8×8×1)	0.100	3.02	18.09 (4.38 THz)	5.5
PBE-GGA (10×10×1)	0.104	3.10	18.04 (4.36 THz)	5.8
HSE06 (8×8×1)	0.168	3.79	18.69 (4.52 THz)	9.0

results from the correction of the self-interaction error within the PBE-GGA functional by the exact exchange contribution of the HSE06 functional [1,7].
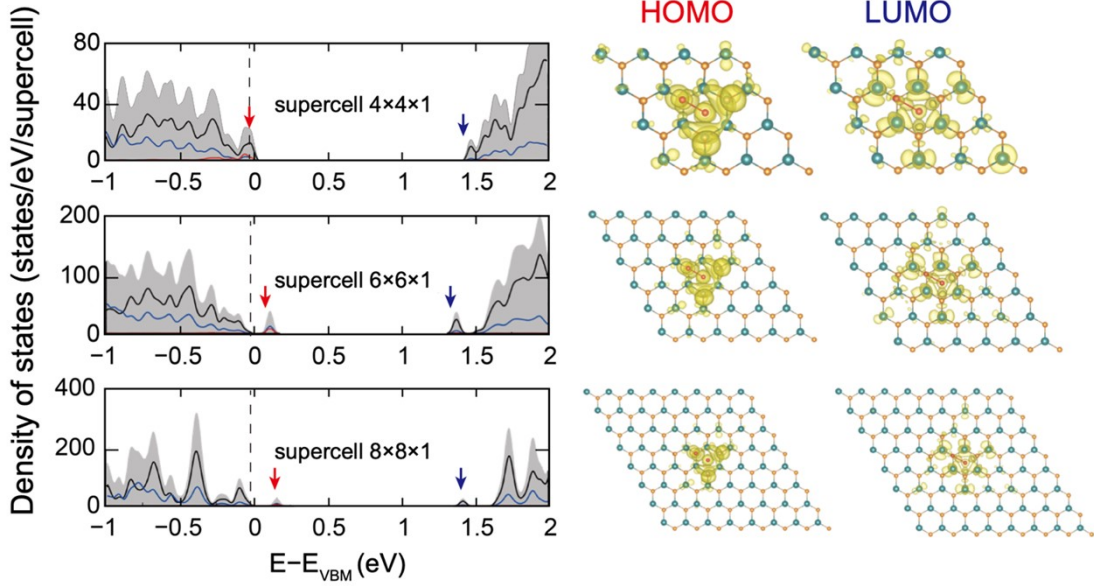
Fig. S2 Density of states (DOS) and partial charge densities of in-gap defect states of $V_{Se}+O_2$ in 4×4×1, 6×6×1, and 8×8×1 monolayer $MoSe_2$ supercells.

IV. Occupation-constrained DFT calculations for the exciton trapped at the $V_{Se}+O_2$ defect complex in monolayer $MoSe_2$

To explain the origins of the experimentally observed defect resonance at 1.72 eV of Fig. 2(a) in the main manuscript, we evaluated the folded oscillator strength (FOS) of the trapped exciton at $V_{Se}+O_2$ defect complex in monolayer $MoSe_2$ calculated with the ΔSCF formalism. Figure S3(a) shows the potential energy surfaces of the exciton trapped at the $V_{Se}+O_2$ defect complex calculated from the ground-state and relaxed excited-state atomic structures. We applied an upward 0.3 eV constant energy shift to the energy surface of the trapped exciton to reflect the underestimation of the quasiparticle gap within our HSE06 calculations. The FOS of the trapped exciton state with the ground and the relaxed structure (Q_g and Q_e) and their difference are presented in Figs. S3(b) and S3(c). As shown in Fig. S3(c), the structural deformations in the ground and the relaxed structures of the $V_{Se}+O_2$ defect complex (from Q_g and Q_e) with the vibration frequency 4.5 THz induces the change of absorption spectra of FOS around 1.73 eV, which
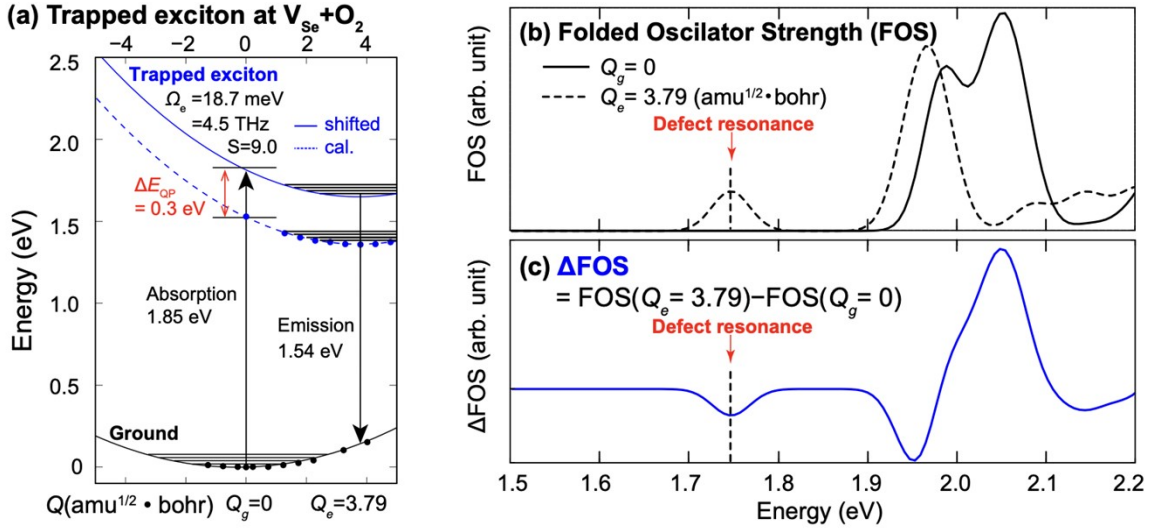
Fig. S3. The evaluation of the folded oscillator strength (FOS) from first-principles calculation data. (a) Initially, ground-state (black circles) and excited-state (blue circles) potential energy surfaces of the $V_{Se}+O_2$ defect complex were calculated using the ΔSCF method [reproduced from Fig. 4(b) of the main manuscript]. The dashed blue line is the harmonic fitting of ΔSCF calculation results, and the solid blue line is the rigid upward shift by $\Delta E_{QP} = 0.3$ eV that reflects the underestimation of the quasiparticle gap of monolayer $MoSe_2$ with respect to the experimental value. (b) The FOSs or absorption spectra were then calculated for the trapped exciton in the ground-state ($Q_g = 0$) and relaxed excited-state atomic structures ($Q_e = 3.79$) with the inclusion of a constant energy shift of 0.3 eV. (c) The difference between the two FOSs evaluated in (b).

corresponds to the defect resonance in experiment observed with 4.5 THz peak. Here, we note that the peak position of 1.73 eV in the difference between two FOSs (ΔFOS) [see Fig. S3(c)] roughly corresponds to the average of absorption and emission energies from the ground-state DFT and excited-state ΔSCF calculations, respectively, i.e., (1.85 eV + 1.54 eV)/2 = 1.70 eV [see Fig. S3(a)].
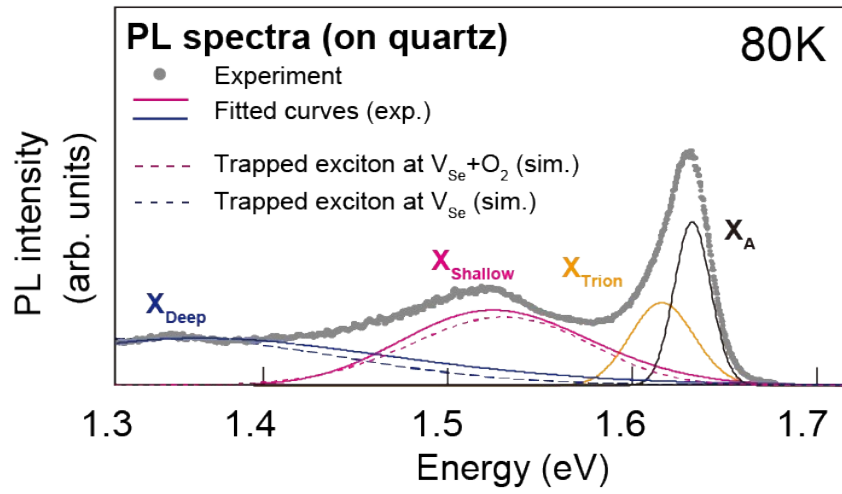
Fig. S4. The experimental PL spectra (in 80K) shown together with the simulated spectra obtained from excitons trapped at $V_{Se}+O_2$ and $V_{\underline{Se}}$ in $MoSe_2$, which are attributed to ST ($X_{Shallow}$) and DT (X_{Deep}), respectively.

References

[1] J. Heyd and G. E. Scuseria, Efficient hybrid density functional calculations in solids: Assessment of the Heyd-Scuseria-Ernzerhof screened Coulomb hybrid functional, *J. Chem. Phys.* **121**, 1187 (2004).

[2] G. Kresse and J. Furthmüller, Efficiency of ab-initio total energy calculations for metals and semiconductors using a plane-wave basis set, *Comput. Mater. Sci.* **6**, 15 (1996).

[3] G. Kresse and J. Furthmüller, Efficient iterative schemes for ab initio total-energy calculations using a plane-wave basis set, *Phys. Rev. B* **54**, 11169 (1996).

[4] J. P. Perdew, K. Burke, and M. Ernzerhof, Generalized gradient approximation made simple, *Phys. Rev. Lett.* **77**, 3865 (1996).

[5] Q. Zheng, VaspBandUnfolding (https://github.com/QijingZheng/VaspBandUnfolding, 2020).

[6] K. Momma and F. Izumi, VESTA 3 for three-dimensional visualization of crystal, volumetric and morphology data, *J. Appl. Crystallogr.* **44**, 1272 (2011).

[7] Y.-H. Kim, M. Städele, and R. M. Martin, Density-Functional Study of Small Molecules within the Krieger-Li-Iafrate Approximation, *Phys. Rev. A* **60**, 16 (1999).